ARTICLE

Minimum lap time trajectory optimization of performance vehicles with four-wheel drive and active aerodynamic control

Pieter de Buck[a] and Joaquim R. R. A Martins[a]

[a]Department of Aerospace Engineering, University of Michigan, Ann Arbor, Michigan, USA

ARTICLE HISTORY
Compiled November 8, 2023

ABSTRACT
As racing vehicles become more complex, optimizing the interaction between subsystems becomes critical for racing performance. In this work, we incorporate two such subsystems into a vehicle model. We investigate the performance benefits of a four-wheel-drive vehicle with independent control over its in-hub motors and active control on the rear wing flap rotation. The performance is evaluated by solving minimum lap time optimal control problems (OCP) for various vehicle configurations. The OCP is transformed into a nonlinear programming problem through direct collocation and is solved by an interior point method. The four-wheel-drive configuration performs better than rear-wheel drive in terms of lap time, finishing the Barcelona circuit 4% faster. The benefits come mainly from higher longitudinal accelerations. Active aerodynamic control improves performance regardless of the propulsion configuration, leading to another 1% of lap time improvement on the Barcelona circuit. The optimal aerodynamic control strategy is different between propulsion configurations, particularly on corner exits. This model enables the exploration of optimal torque vectoring controls and their interaction with a vehicle's active aerodynamics. This is needed to guide the design of the increasingly complex racing vehicle controllers of the future.

KEYWORDS
optimal control; trajectory optimization; racing; 4WD; active aerodynamics; electric vehicles

1. Introduction

Race car performance optimization by solving minimum lap time problems is an invaluable tool for the engineering design process. Without going to the track, engineers can evaluate trade-offs between vehicle design parameters and ultimately choose a design that meets their specific needs. Additionally, the optimal vehicle configuration changes based on the specific track layout, weather, and surface conditions. Knowing how the vehicle responds in various scenarios is imperative for a winning race strategy.

As the automotive industry moves towards widespread electrification of vehicles, automotive racing is following this trend. Series such as Formula E are rapidly gaining traction, and the vehicle's performance is steadily increasing. Electric race cars are positioned to introduce significant technological advances to motorsport, and innovations in this space could be adopted in electric passenger vehicle design. Four-wheel drive

CONTACT Pieter de Buck. Email: pdebuck@umich.edu

vehicles driven by electric in-hub motors can exploit sophisticated control strategies to best use their instantaneous torque response and energy recuperation capabilities. Vehicles with active aerodynamic control can trade off cornering performance for straight-line speed during the lap.

These innovations require detailed and accurate lap time simulation to guide the engineering design. Scherenberg [19] first applied lap time simulation to find the optimal gearing and bodywork shape for a specific circuit. Nowadays, lap time simulation methods are ubiquitous.

To solve the minimum lap time problem, authors have employed fixed-trajectory, quasi-steady-state solutions [22,23]. While this approach is computationally efficient, it requires the "racing line" as an input to the problem. Because the racing line depends on the vehicle [18] and road conditions [25,26], it needs to be guessed. Strategies for obtaining the racing line include using GPS telemetry from on-track testing and performing simplified analysis such as computing minimum-distance or minimum-curvature paths [1].

To solve for the optimal vehicle controls in quasi-steady fixed trajectory problems, the general strategy is to solve for the acceleration zones by stepping forward in time, then solve for the braking zones in reverse. The optimal solution is then found by taking the minimum velocity of those two solutions. The quasi-steady strategy is useful because it is simple and computationally efficient. This allows vehicle parameter sweeps that serve as baseline results for more sophisticated analysis or general vehicle design targets. The drawbacks of this approach include the lack of modeling of the transient response of the suspension system and other transient phenomena, such as tire wear and tire temperature shifts. Additionally, the solution is sub-optimal in most cases because the racing line is an input to the analysis.

Since then, more sophisticated implementations of lap time simulation have included optimization of the vehicle trajectory by formulating the problem as an optimal control problem (OCP). Using this technique, the minimum lap problem has been solved in conjunction with optimal vehicle parameters [18,26], hybrid energy recovery systems [13], aero-suspension interactions [10], tire usage [28], and varying road surface properties [3,25]. Sharp and Peng [21] performed a comprehensive review of minimum lap time methods and other applications of automotive optimal control. A decade later, Massaro and Limebeer [15] included recent developments in the field in another review.

The works cited above have focused on optimizing vehicle systems already used in racing. Gaps in the literature exist in novel technologies that could be implemented in future racing series. In this work, we analyze how precise control over four in-hub motors compares against two-wheel-drive and four-wheel-drive vehicles without individual control over each wheel. Optimal control of the four-wheel drive with in-hub motors configuration has primarily been investigated through the lens of stability and controllability of passenger vehicles [2,6], instead of racing applications. When operating on the limit of power and traction, the vehicle's behavior and the goal of the optimization problem are vastly different. We have to consider additional constraints, such as the maximum motor power or tire adherence, which are generally not applicable to passenger vehicles.

In four-wheel-drive minimum lap time problems, torque vectoring controllers have been designed to leverage the four in-hub motors providing individual acceleration and braking responses [5,24]. These controllers are essential for implementing control strategies for vehicles with this propulsion configuration. However, these studies were limited to single hairpin or partial track maneuvers. Heilmeier et al. [8] pro-

vides an example of full track trajectory planning, which is accomplished by finding the minimum-curvature path. Similar to a previous investigation of optimal energy recuperation in Formula 1 vehicles by Limebeer et al. [13], Sedlacek et al. [20] solved minimum lap time problems for four-wheel drive electric vehicles considering battery pack and motor performance dynamics. Otherwise, as noted by De Castro et al. [5], the space of four-wheel-drive electric vehicle lap time optimization is limited.

In addition to investigating four-wheel-drive performance, we examine the benefits of active control of a rear wing flap rotation. This resembles the drag reduction system (DRS) found on Formula 1 cars. However, in this case, the control is varied continuously within the allowable range of motion throughout the lap, as opposed to being open or closed in specific sections of the track. We use experimental wind tunnel data from Jeffrey et al. [11] to establish the relationship between the rear wing aerodynamic coefficients and rotation of the flap. Imani Masouleh and Limebeer [10] performed a similar analysis by allowing the aerodynamic balance of the vehicle to change during the lap continuously. They found that this hypothetical control leads to substantial balance shifts during the lap. However, the range of the balance control is not achievable for a vehicle with actively controlled aerodynamic surfaces. By incorporating experimental data into the vehicle model, this work aims to find the effect of aerodynamic balance shifts with a realistic control range. The present work expands on previous investigations by finding the optimal trajectory of a four-wheel-drive electric vehicle for entire race tracks and an actively controlled rear wing flap.

2. Problem formulation

2.1. Optimal Control Problem

The OCP is formulated and solved using the multidisciplinary design optimization (MDO) framework OpenMDAO [7], combined with the optimal control package Dymos [**?**]. This package extends the capabilities of the OpenMDAO framework by allowing the user to input the governing state equations and their derivatives in a modular fashion. The phases of the OCP are discretized onto a grid of state, control, and collocation nodes, turning the OCP into a nonlinear programming (NLP) problem.

This work uses the Legendre–Gauss–Lobatto transcription technique to perform this discretization. Table 1 shows the formulation of the OCP. The vehicle is placed under cyclic constraints, meaning that the states are continuous between the start and end of the lap. Path constraints ensure that the tires stay within their friction limits and that the power limit of the vehicle is respected, while variable bounds constrain the states. The system dynamics and constraints are detailed in Section 2.2.

2.2. System Dynamics

The vehicle model for this work is a 3-DOF model adapted from Dal Bianco et al. [4]. The model is adapted to include aerodynamic downforce for the vehicle and controllable rear wing, as well as modifications to allow for various propulsion configurations. Additionally, the independent variable is changed from time t to the distance along the centerline s, which is common in minimum lap time problems. This is detailed in Section 2.3. The three DOF are the vehicle velocity V, the slip angle λ, and the yaw rate Ω. To approximate the transient suspension effects, the longitudinal and lat-

Table 1. Optimization problem formulation.

		Symbol	Lower	Upper	Units
minimize	Time	t			s
by varying					
controls	Front left thrust	T_{fl}			
	Front right thrust	T_{fr}			
	Rear left thrust	T_{rl}			
	Rear right thrust	T_{rr}			
	Rear wing flap angle	γ	0	50	deg
	Steering angle	δ			rad
states	Speed	V			$\mathrm{m\,s^{-1}}$
	Longitudinal acceleration	a_x			$\mathrm{m\,s^{-2}}$
	Lateral acceleration	a_y			$\mathrm{m\,s^{-2}}$
	Normal distance to centerline	n	-4	4	m
	Angle relative to centerline	α			rad
	Slip angle	λ			rad
	Yaw rate	Ω			$\mathrm{rad\,s^{-1}}$
subject to	Front left adherence	c_{fl}	0	1	
	Front right adherence	c_{fr}	0	1	
	Rear left adherence	c_{rl}	0	1	
	Rear right adherence	c_{rr}	0	1	
	Front left power	P_{fl}		75	kW
	Front right power	P_{fr}		75	kW
	Rear left power	P_{rl}		75	kW
	Rear right power	P_{rr}		75	kW
	Periodic state constraints				
	System dynamics as collocation constraints				
	Track layout				

eral vehicle accelerations a_x and a_y are treated with a low pass filter [4]. The track is represented in a curvilinear coordinate system, as is common in optimal vehicular control [14].

The three states that govern the vehicle's position relative to the track are the distance along the centerline s, the vehicle angle relative to the track centerline α, and the vehicle distance normal to the centerline n. Given a track width of eight meters, the magnitude of n is bounded to be less than four meters, which keeps the vehicle within the track boundaries. The steering angle δ is one of the OCP controls. The track is constructed by defining a sequence of straight segments (with a certain length) and corners (with a certain radius, sweep, and direction). This allows for an approximate representation of any racetrack. The curvature κ is found by fitting the resulting track centerline to a quintic spline. Using the parametric representation of the spline $x(s), y(s)$, where s is the distance along the centerline, the curvature is given by

$$\kappa = \frac{x'y' - y'x''}{\left(x'^2 + y'^2\right)^{3/2}}. \tag{1}$$

The vehicle geometric parameters and tire forces are shown in Figure 1. The vehicle position relative to the track centerline and vehicle degrees of freedom is shown in

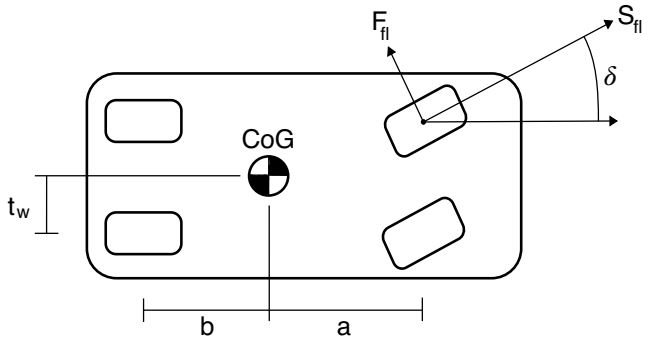

Figure 1. Vehicle geometric parameters and tire forces.

Figure 2. The 3-DOF car model with the curvilinear track approximation is as follows:

$$\begin{aligned}
\dot{s} &= \frac{V\cos(\alpha-\lambda)}{1-n\kappa} \\
\dot{n} &= V\sin(\alpha-\lambda) \\
\dot{\alpha} &= \Omega - \frac{\kappa V\cos(\alpha-\lambda)}{1-n\kappa} \\
M\Omega V\lambda + M\dot{V} &= S_{rr}+S_{rl}+S_{fr}+S_{fl}-\delta(F_{fr}+F_{fl})-D_{\text{vehicle}}-D_{\text{wing}} \\
M(\Omega V-\dot{V}\lambda-V\dot{\lambda}) &= \delta(S_{fr}+S_{fl})+F_{rr}+F_{rl}+F_{fr}+F_{fl} \\
I_z\dot{\Omega} &= a(F_{fr}+F_{fl})-b(F_{rr}+F_{rl})+t_w(-S_{rr}+S_{rl}-S_{fr}+S_{fl}),
\end{aligned} \tag{2}$$

where F_{ij} and S_{ij} are the tire lateral and longitudinal forces, respectively. D_{vehicle} and D_{wing} are the aerodynamic drag of the vehicle and rear wing, respectively. I_z is the yaw inertia of the vehicle and M is the mass. The states and vehicle parameters are also defined in Tables 1 and 2.

The normal forces of the tires are defined as

$$\begin{aligned}
N_{rr} &= \frac{Mg}{2}\frac{a}{a+b}+\frac{M}{4}\left(\frac{a_x h}{a+b}-a_y(1-\chi)\frac{h}{t_w}\right)+\frac{L_{\text{vehicle}}}{2}\frac{\text{CoP}}{a+b}+\frac{L_{\text{wing}}}{2} \\
N_{rl} &= \frac{Mg}{2}\frac{a}{a+b}+\frac{M}{4}\left(\frac{a_x h}{a+b}+a_y(1-\chi)\frac{h}{t_w}\right)+\frac{L_{\text{vehicle}}}{2}\frac{\text{CoP}}{a+b}+\frac{L_{\text{wing}}}{2} \\
N_{fr} &= \frac{Mg}{2}\frac{b}{a+b}+\frac{M}{4}\left(-\frac{a_x h}{a+b}-a_y\chi\frac{h}{t_w}\right)+\frac{L_{\text{vehicle}}}{2}\left(1-\frac{\text{CoP}}{a+b}\right) \\
N_{fl} &= \frac{Mg}{2}\frac{a}{a+b}+\frac{M}{4}\left(-\frac{a_x h}{a+b}+a_y\chi\frac{h}{t_w}\right)+\frac{L_{\text{vehicle}}}{2}\left(1-\frac{\text{CoP}}{a+b}\right),
\end{aligned} \tag{3}$$

where L_{vehicle} and L_{wing} are the aerodynamic downforce generated by the vehicle and rear wing, respectively. The vehicle's center of pressure (CoP) coincides with the center of gravity. The rear wing forces act directly at the rear wheels, effectively moving the center of pressure aft, depending on the vehicle velocity. Velocity-dependent lift and drag coefficient curves for the vehicle were obtained from Limebeer and Perantoni [12], where the vehicle's frontal area is set to 1 m^2. g is standard gravity. The height of the CoG off the ground is h. χ is the front-to-rear roll balance.

The flap angle (γ) dependent wing aerodynamic coefficients were obtained from

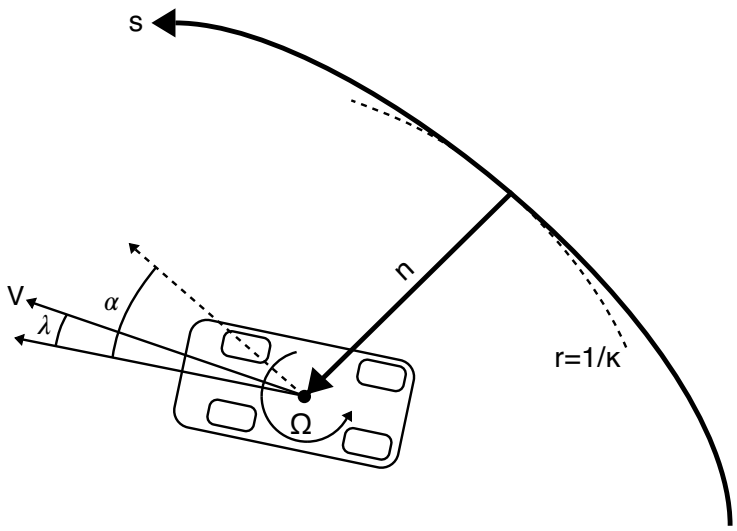

Figure 2. Vehicle position relative to the track centerline and vehicle degrees of freedom.

Jeffrey et al. [11], where the mainplane angle of attack is set to zero degrees. The flap angle control is bound to be between zero and fifty degrees. A linear relationship between flap angle and coefficients is assumed, which results in the following expressions for the vehicle and wing downforce and drag:

$$\begin{aligned} C_D A &= 1.055 - 7.588 \times 10^{-4} V - 9.156 \times 10^{-6} V^2 \\ C_L A &= 1.614 - 1.361 \times 10^{-3} V - 4.186 \times 10^{-5} V^2 \\ C_{\mathrm{D,wing}} &= 0.0667 + 0.0127\gamma \\ C_{\mathrm{L,wing}} &= 1.5833 + 0.0333\gamma \\ L_{\mathrm{vehicle}} &= \frac{1}{2}\rho C_L A V^2 \\ D_{\mathrm{vehicle}} &= \frac{1}{2}\rho C_D A V^2 \\ L_{\mathrm{wing}} &= \frac{1}{2}\rho C_{L_w} S_w V^2 \\ D_{\mathrm{wing}} &= \frac{1}{2}\rho C_{D_w} S_w V^2. \end{aligned} \tag{4}$$

The tire forces are obtained differently depending on the propulsion configuration. For a rear-wheel-drive vehicle, we have a single thrust control T, where T^+ and T^- return the positive or negative values, respectively. This is equivalent to $T^+ = \max(0, T)$ and $T^- = \min(0, T)$. The torque is equal between the left and right sides of the vehicle, which is equivalent to an open differential. The $Mg/2$ term normalizes the control values such that the magnitude is $\mathcal{O}(1)$. Given a brake bias β, we define:

$$S_{fl} = S_{fr} = \frac{Mg}{2} T^- \beta, \qquad S_{rl} = S_{rr} = \frac{Mg}{2}\left(T^+ + T^-(1-\beta)\right). \tag{5}$$

For a four wheel drive vehicle with a single thrust control, we assume a 50/50 tractive

force distribution between the front and rear axles. The equation is given as:

$$S_{fl} = S_{fr} = \frac{Mg}{2}\left(T^{+} + T^{-}\beta\right), \qquad S_{rl} = S_{rr} = \frac{Mg}{2}\left(T^{+} + T^{-}(1-\beta)\right). \tag{6}$$

Finally, for a four wheel drive vehicle with individual controls for each wheel's thrust, the longitudinal forces are:

$$S_{fl} = S_{fr} = S_{rl} = S_{rr} = \frac{Mg}{2}\left(T^{+} + T^{-}\right). \tag{7}$$

The lateral forces of the tire are dependent on the slip angle of each individual tire (λ_{ij}). Given a tire cornering stiffness per unit load K_λ, we define the forces as

$$F_{ij} = N_{ij} K_\lambda \lambda_{ij}, \tag{8}$$

where the tire slip angles are:

$$\begin{aligned} \lambda_{rr} &= \lambda + \frac{\Omega(b + \lambda t_w)}{V}, & \lambda_{fr} &= \lambda + \delta - \frac{\Omega(a - \lambda t_w)}{V} \\ \lambda_{rl} &= \lambda + \frac{\Omega(b - \lambda t_w)}{V}, & \lambda_{fl} &= \lambda + \delta - \frac{\Omega(a + \lambda t_w)}{V}. \end{aligned} \tag{9}$$

Using the tire forces F_{ij} and S_{ij}, we define the tire adherence constraints c_{ij}, which ensure that the tires stay within the friction ellipse defined by

$$\begin{aligned} c_{ij} &= \left(\frac{S_{ij}}{N_{ij}\mu_{ij}^{x}}\right) + \left(\frac{F_{ij}}{N_{ij}\mu_{ij}^{y}}\right) \\ \mu_{ij}^{x/y} &= \mu_0^{x/y} + K_\mu \frac{N_{ij}}{N_{0,ij}}, \end{aligned} \tag{10}$$

where $N_{0,ij}$ are the static loads based on the center of gravity (CoG) location on each tire, and $\mu_{ij}^{x/y}$ are the lateral and longitudinal tire friction coefficients. While there is some load sensitivity due to the K_μ parameter, this tire model is relatively simple. More sophisticated models such as TMeasy [9] or the Magic Formula [17] could also be used.

As mentioned previously, the time derivatives of the vehicle accelerations are treated with a low pass filter with time constant $\tau_{a_{x/y}}$ to approximate transient suspension effects as

$$\begin{aligned} \tau_{a_x}\dot{a}_x + a_x &= \dot{V} + \Omega V \lambda \\ \tau_{a_y}\dot{a}_y + a_y &= \Omega V - \dot{V}\lambda - V\dot{\lambda}. \end{aligned} \tag{11}$$

2.3. Solution strategy

The open-source interior-point optimizer IPOPT [27] is used to solve the NLP problem, through the pyOptSparse interface [**?**]. This is a robust method with reasonable wall times. Figure 3 shows a study based on the four-wheel-drive vehicle with individual

Table 2. Vehicle Parameters.

Parameter	Value	Units	Description
M	1184	kg	Vehicle mass
a	1.404	m	CoG to front axle distance
b	1.356	m	CoG to rear axle distance
t_w	0.807	m	Half track width
h	0.4	m	CoG height
I_z	1775	$\mathrm{kg\,m^2}$	Yaw inertia
β	0.62	–	Brake balance
χ	0.5	–	Roll balance
ρ	1.2	$\mathrm{kg\,m^{-3}}$	Air density
μ_0^x	1.68	–	Longitudinal base friction coefficient
μ_0^y	1.68	–	Lateral base friction coefficient
K_μ	-0.5	–	Tire load sensitivity
K_λ	44	–	Tire cornering stiffness per unit load
τ_{a_x}	0.2	s	Longitudinal load transfer time constant
τ_{a_y}	0.2	s	Lateral load transfer time constant
S_w	0.8	$\mathrm{m^2}$	Wing planform area
CoP	1.404	m	Center of pressure to front axle distance

thrust controls on the Barcelona track, with third-order segments. The final data point corresponds to a problem size of 1300 segments. The discretization for the optimization problem uses 800 third-order Gauss–Lobatto segments to save computational time. This discretization corresponds to a grid spacing of 3 meter. The order of the segments is constant, and the length of the segments is equal.

States, controls, constraints, and the objective function are scaled to ensure they are $\mathcal{O}(1)$ when sent to IPOPT. IPOPT is configured to not perform any internal scaling. We found a critical IPOPT setting to be `mu_init`, which is the initial value of the barrier parameter. For this application, we found that lowering that initial value from 10^{-1} to 10^{-3} significantly affects the convergence speed and stability. The default setting does not allow the solver to get close enough to the track width and traction limits to make any meaningful progress to an optimum solution. Relaxing that initial barrier slightly leads to more reliable solver behavior.

An essential aspect of the solution strategy is the choice of the independent variable. The work that is the source of the vehicle model provides the state equations as functions of time [4]. In this work, those state equations are transformed to be a function of the distance along the centerline of the track s. This is possible when s increases monotonically with t, which is always the case for this problem. This transformation is performed in a similar fashion as Lot and Biral [14] and is given by

$$\begin{aligned} \dot{s} &= \frac{ds}{dt} = \frac{V\cos\alpha - \lambda}{1 - n\kappa}, \\ n' &= \frac{dn}{ds} = \frac{\dot{n}}{\dot{s}}. \end{aligned} \tag{12}$$

This transformation is carried out for each state equation (2). The advantage is that the OCP is discretized in space instead of time. For time-based problems, shifting collocation nodes in space leads to convergence issues and numerical difficulties. Moreover, bypassing the free final time issue inherent in time-based problems is advantageous.

The largest optimization problem (four-wheel drive with individual thrust controls and active aerodynamics) converges in 36.7 minutes on a computer with an Intel i9 2.3 GHz processor and 32 GB of memory.

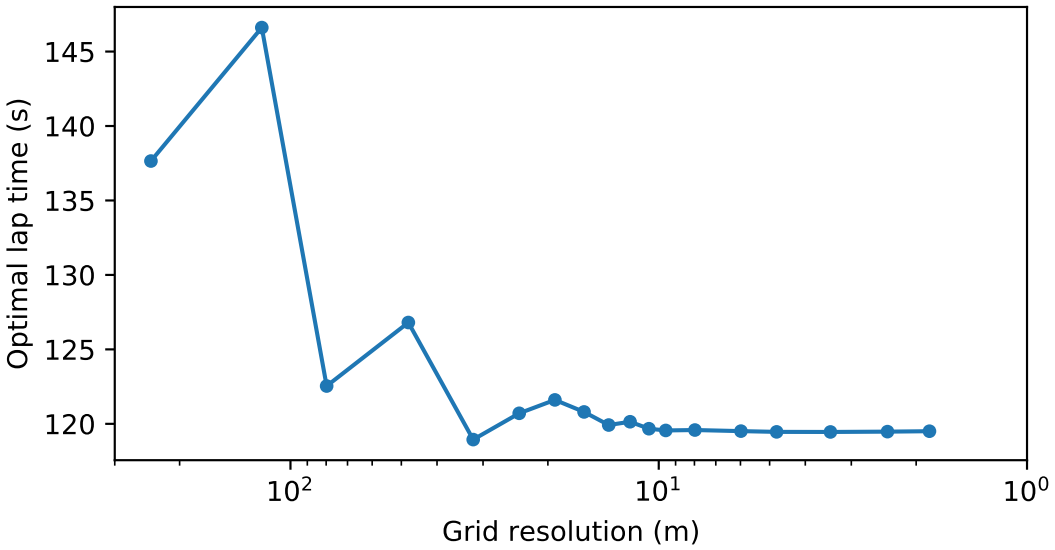

Figure 3. Optimal lap time for various values of grid spacing.

3. Results

We compare vehicle models that differ in their propulsion configuration and aerodynamics controls. We examine a rear-wheel-drive vehicle with a single thrust control, a four-wheel-drive vehicle with a single thrust control, and a four-wheel-drive vehicle with individual wheel thrust controls (in-hub motors). Additionally, we distinguish between active control of the rear wing flap angle and a fixed flap angle. Regardless of the propulsion setup, the total power available at the wheels is 300kW.

Table 3 shows the lap times for various propulsion and aerodynamics configurations. The optimization is performed on the Barcelona track discretized on a grid with 800 grid segments, representing a three-meter grid spacing between nodes. Regardless of whether the aerodynamic control is active or not, we see that the rear-wheel-drive vehicle is the slowest, followed by the four-wheel-drive vehicle with a single thrust control and the four-wheel-drive vehicle with individual thrust controls. For each of the three propulsion configurations, the difference in lap time between the fixed and active aerodynamics is relatively similar. The rear-wheel drive vehicle is 1.292s (1.04%) faster with active aerodynamics, compared to 1.371s (1.12%) and 1.417s (1.19%) faster for the rear-wheel drive vehicles with single and individual thrust controls, respectively. These represent significant gains in lap time, where a second could mean the difference between the front and back of the pack.

The trajectory for the four-wheel-drive vehicle with in-hub motors colored by velocity is shown in Figure 4, along with labeled corners of the Barcelona track. The vehicle follows an intuitive racing line and accelerates and decelerates appropriately.

When evaluating driver and vehicle performance, they must be operating *on the limit* throughout the lap. This means that the vehicle should be power-limited, traction-limited, or in transition between the two at all times. Figure 5 shows the power limit constraint and the maximum of the four-tire adherence constraints. We can see that the vehicle has active performance constraints for nearly the entire lap, indicating that the optimizer has found a solution that maximizes the vehicle's per-

Table 3. Vehicle configuration lap times.

Propulsion configuration	Aerodynamics control	Lap time (s)
RWD single thrust	Active	124.435
RWD single thrust	Fixed ($\gamma = 50$ deg)	125.727
4WD single thrust	Active	122.046
4WD single thrust	Fixed ($\gamma = 50$ deg)	123.417
4WD individual thrust	Active	119.480
4WD individual thrust	Fixed ($\gamma = 50$ deg)	120.897

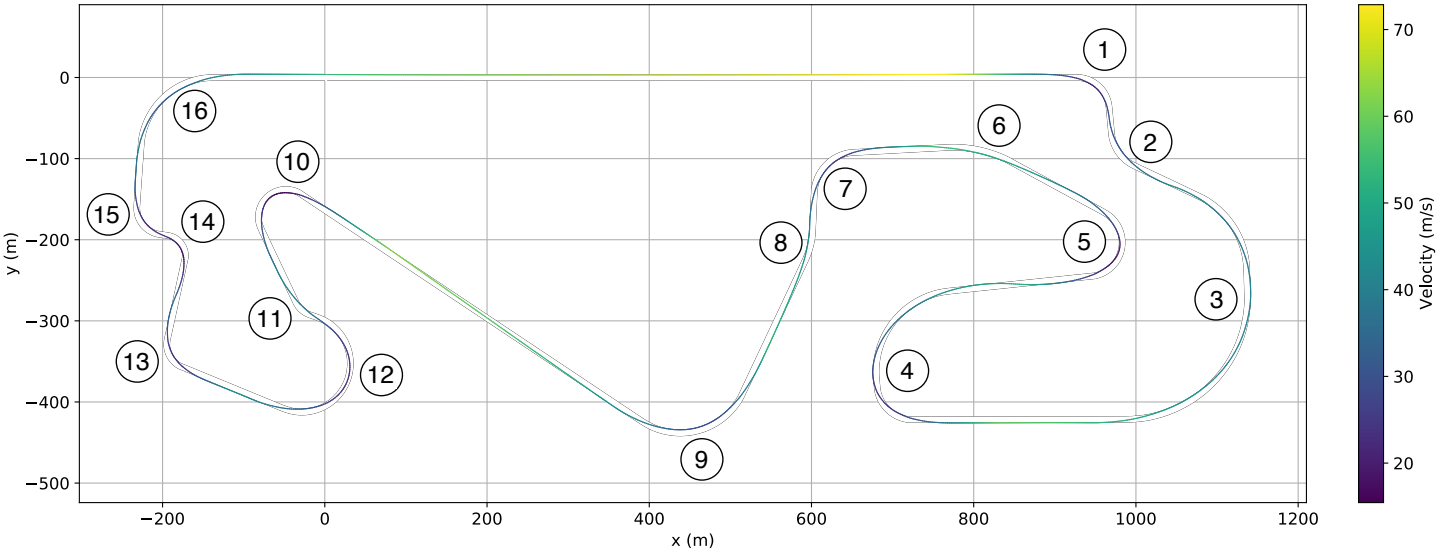

Figure 4. Velocity on Barcelona track for the four-wheel drive vehicle with individual thrust control with turn labels.

formance.

The wing angle control for the four-wheel-drive vehicle with in-hub motors is visible in Figure 6. We notice that the flap angle is increased in the braking zone and throughout the corner. This increase in downforce allows the vehicle to apply more braking and lateral forces. The increase in drag is also beneficial under deceleration. In most corners, the wing angle is reduced to zero degrees at or just after the apex, indicating that additional wing downforce is no longer worth the increased drag.

An interesting feature of the four-wheel-drive vehicle results is that the wing angle control resembles a "bang-bang" control scheme. The wing flap is either fully up or down, except for the sweeping turn 3. The results for the two-wheel-drive vehicle in Figure 7 show a similar control scheme. However, it contains many short actuations of

Table 4. Distance along the centerline to mid-corner for the Barcelona racetrack.

Corner	Distance (m)	Corner	Distance (m)
1	957	9	3063
2	1044	10	3685
3	1318	11	3841
4	1897	12	3959
5	2266	13	4211
6	2491	14	4353
7	2685	15	4408
8	2789	16	4576

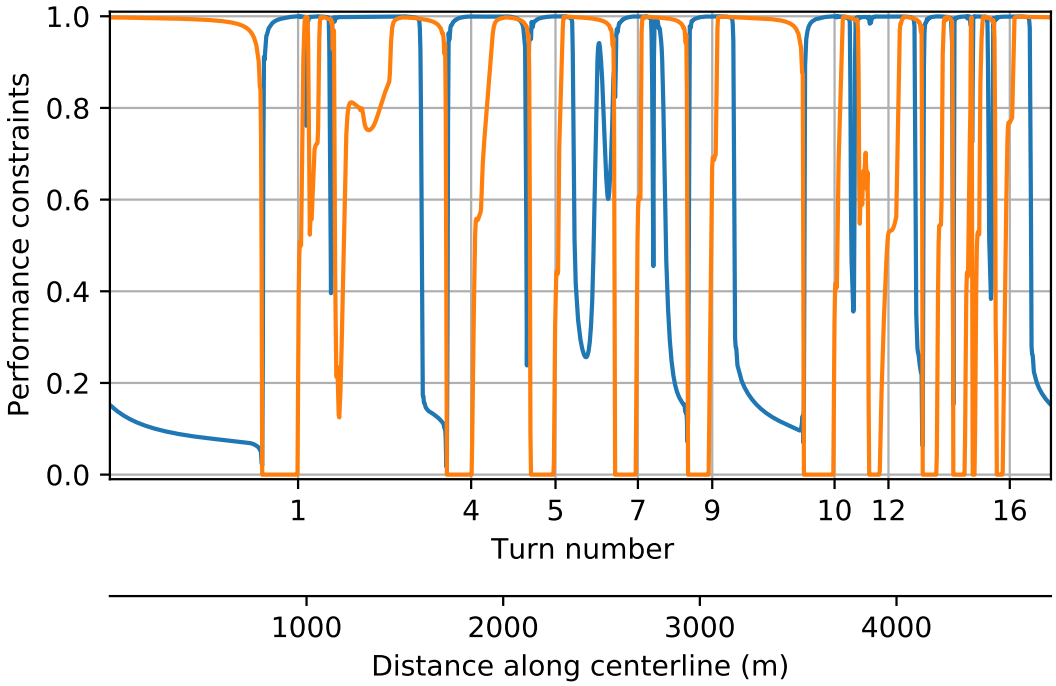

Figure 5. Performance constraints for the four wheel vehicle with individual thrust controls. The blue trace designates the maximum tire adherence constraint of the wheels, while the orange trace designates the maximum power of the in-hub motors as a function of the distance along the centerline of the track.

the rear wing flap, often at corner entry. Additionally, the wing angle control becomes especially erratic in the winding section of the track from turn ten to the finish line. This work does not consider the transient aerodynamic effects of the moving flap. A large scale (fully up to fully down) actuation requires a certain amount of time, followed by another time period where the lift and drag coefficients settle to their steady-state value. If this delay is too significant, the lap time improvement from short decreases in drag might not outweigh the loss in aerodynamic downforce during cornering. Merkel [16] uses Wagner's function combined with servo motor and linkage dynamics to find that servo actuation and flow reattachment occurs after 200 ms. For a conservative average corner speed of 25 m/s, we can compute that the vehicle travels 5 m before the aerodynamic downforce reaches the steady-state value. This means that the rapid wing angle changes during corner entry seen in Figure 7 would not be worthwhile in terms of lap time improvement.

We can take a closer look into the differences between the various vehicle configurations by examining data traces for each of their laps. Figure 8 shows how the four-wheel-drive vehicle with individual thrust control stacks up against the two-wheel-drive vehicle. Both have active aerodynamics, evidenced by the varying wing angle during the lap. The velocity trace shows that the four-wheel-drive vehicle brake later and has a lower minimum cornering speed than the two-wheel-drive vehicle. Because of the individual control over each wheel's throttle and braking, the four-wheel-drive vehicle gets closer to the adherence limit for each tire. This allows it to accelerate and decelerate significantly quicker than the two-wheel-drive vehicle, which is limited to rear-wheel only propulsion under acceleration and four-wheel braking with a certain braking bias under deceleration. Even though the four-wheel-drive vehicle takes the

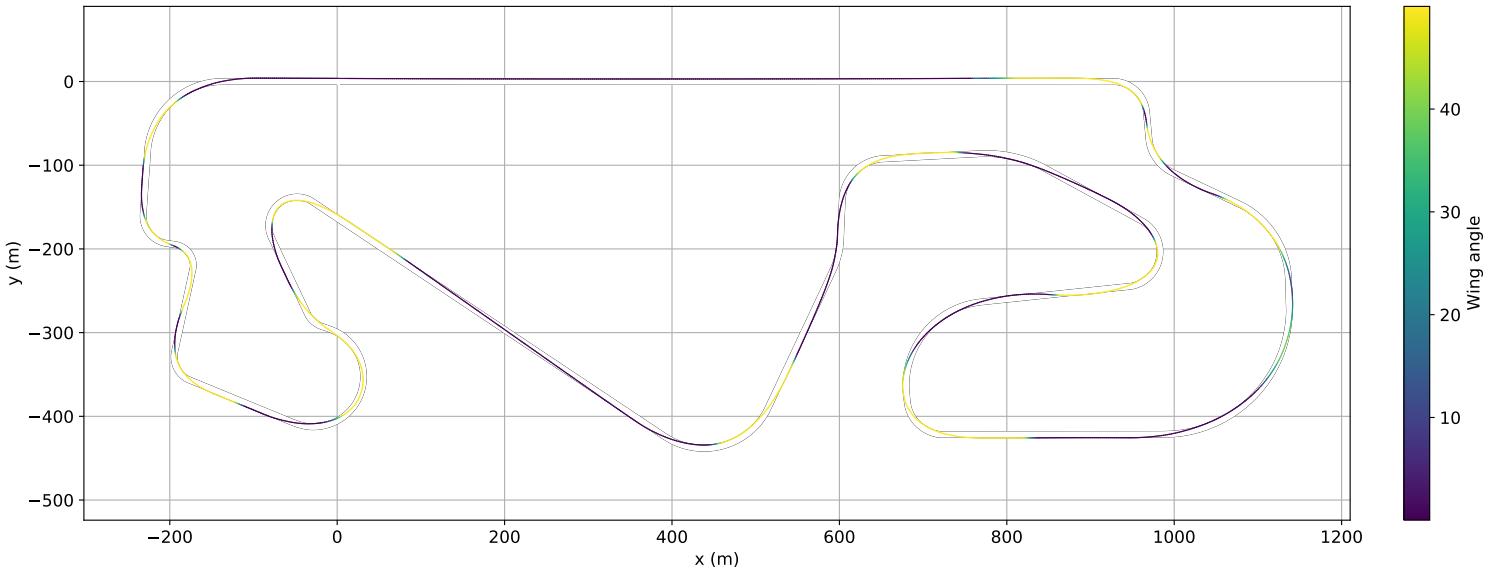

Figure 6. Wing angle on Barcelona track for the four-wheel drive vehicle with individual thrust control.

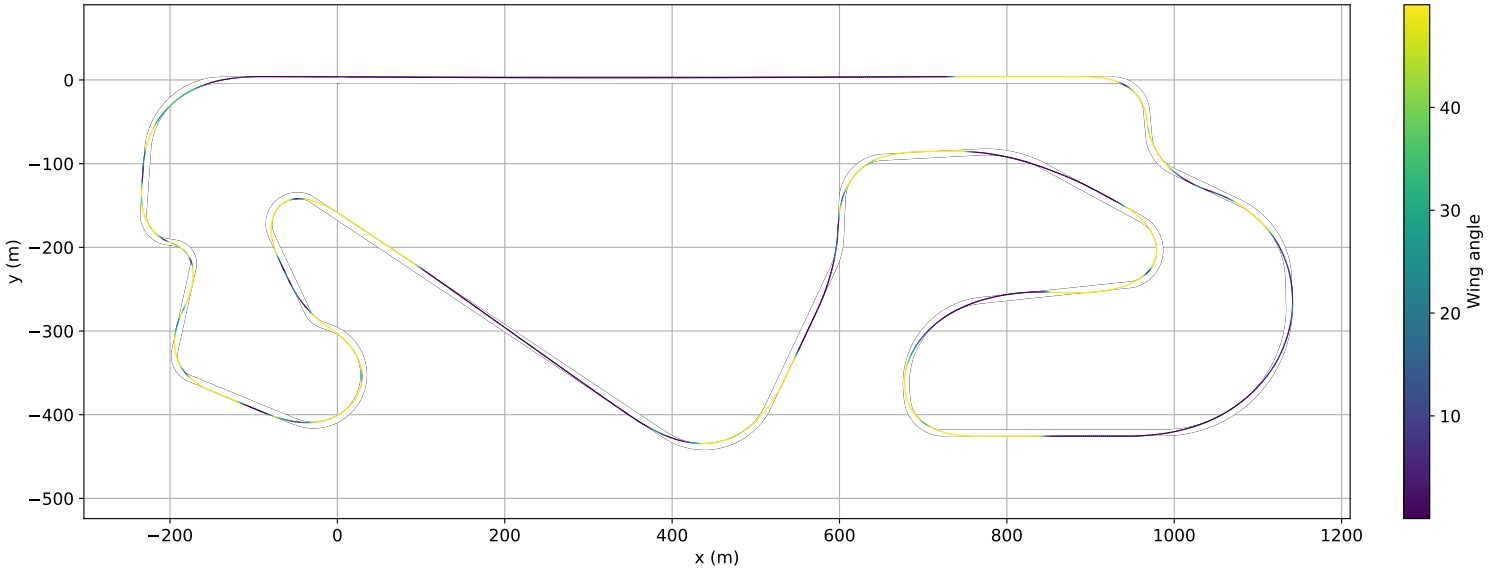

Figure 7. Wing angle on Barcelona track for the two-wheel drive vehicle.

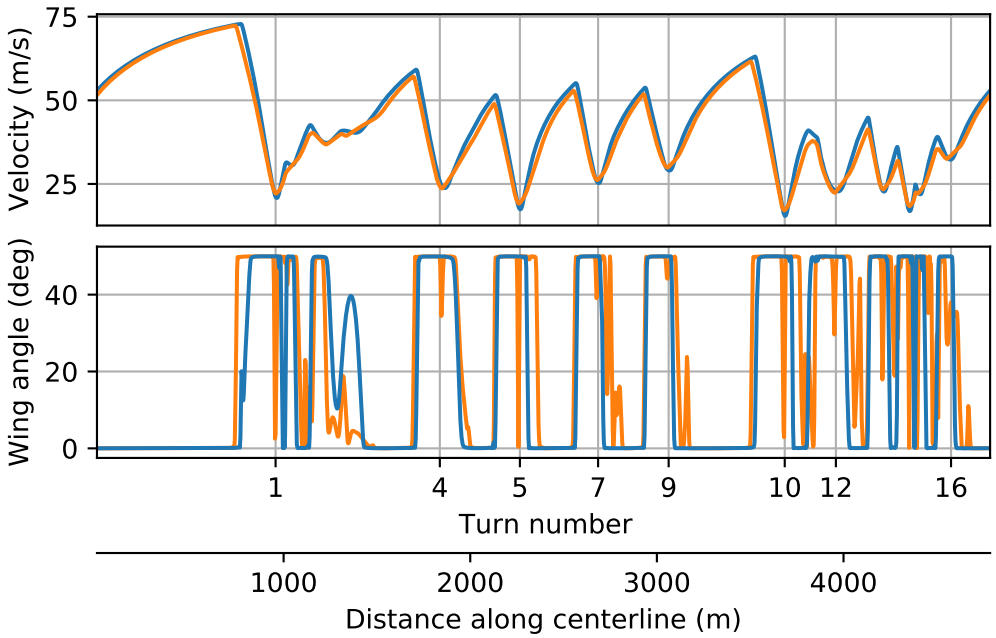

Figure 8. Four-wheel drive with active aerodynamics (blue line) compared with two-wheel drive with active aerodynamics (orange line) on the Barcelona track. The lower graph shows the wing angle of each vehicle.

corner apex at a lower speed, it quickly makes that up in the following acceleration zone. This indicates that the four-wheel-drive vehicle prefers to get fully turned in, with lower lateral forces on the tires, before applying maximum throttle to all wheels. On the other hand, the two-wheel-drive vehicle prefers to keep its speed up throughout the corner, requesting larger lateral forces from the tires. This resembles a driving style one would utilize in karts or in wet conditions, where acceleration and deceleration performance is diminished relative to cornering performance, making it preferable to keep momentum up during the lap. Smith et al. [24] found similar results, where a four-wheel-drive vehicle with individual thrust controls has a lower minimum cornering speed than a four-wheel-drive vehicle with a single thrust control while still completing the U-turn maneuver much quicker. Our results expand on that work by showing the same phenomenon on an entire racetrack, with more varied corner geometries and entry and exit conditions. De Castro et al. [5] also found similar results for a single U-turn maneuver. Their optimal torque allocation strategy for a four-wheel-drive vehicle with individual thrust controls resembles the results in this work. The vehicle has an *understeering yaw moment* upon corner entry, followed by an *oversteering yaw moment* on corner exit. Our results show this over the entire racetrack and integrate it with active aerodynamic control.

From the wing angle traces, it is clear that both vehicle configurations have that "bang-bang" control scheme that was discussed previously. The two-wheel-drive vehicle increases the wing angle to the maximum before the four-wheel-drive vehicle and lowers it back down to the lowest drag configuration after the four-wheel-drive vehicle. This is related to the analysis in the previous paragraph because the four-wheel-drive vehicle brakes later and can achieve a higher yaw rate through torque vectoring. Turn five, in particular, shows how much longer the two-wheel-drive vehicle uses the increased aerodynamic downforce to round the corner.

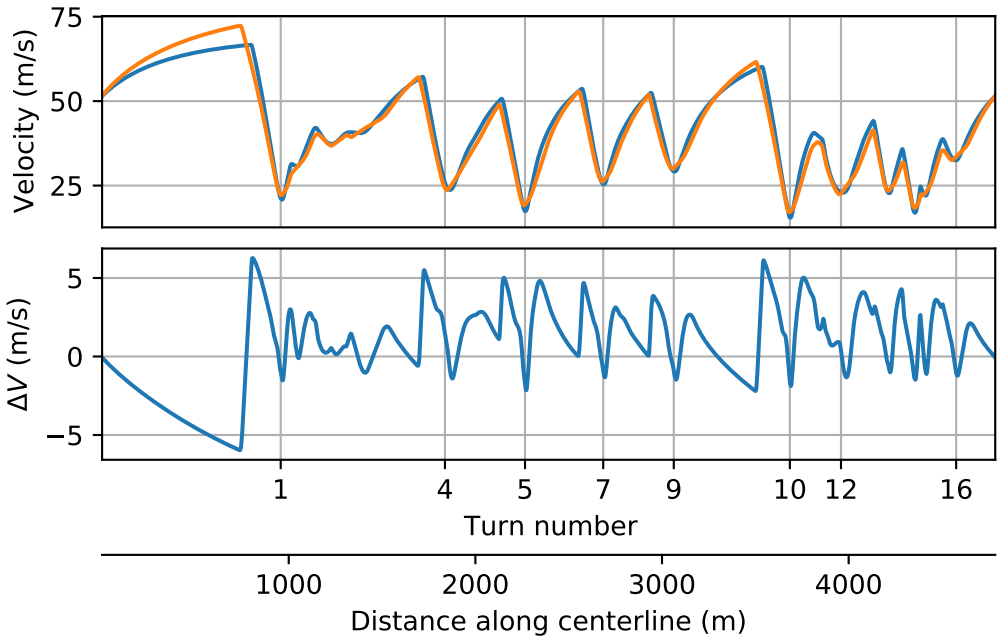

Figure 9. Four-wheel drive with fixed aerodynamics (blue line) compared with two-wheel drive with active aerodynamics (orange line) for the Barcelona track. The lower graph shows the velocity difference $\Delta V = V_{4\text{WD}} - V_{2\text{WD}}$.

Figure 9 compares the data between a two-wheel-drive vehicle with active aerodynamics and the four-wheel-drive in-hub motor vehicle with the rear wing flap fixed in the high downforce configuration. Even though the two-wheel-drive vehicle has a large speed advantage on the straights because of its drag reduction capability, the four-wheel drive vehicle is roughly 3.5s faster over the lap. We can make similar observations to the previous comparison. The four-wheel-drive vehicle has a lower minimum cornering speed but accelerates much quicker on corner exits, as evidenced by the ΔV trace. However, it cannot keep this advantage for long because the two-wheel-drive vehicle catches back up on straight sections. Still, the ability of the four-wheel-drive vehicle to saturate each wheel's adherence under throttle and braking leads to a significant advantage over the lap. Table 3 shows us that even the four-wheel-drive vehicle with a single thrust control is faster than the two-wheel-drive vehicle. This indicates that the two-wheel-drive vehicle is severely limited by load transfer and could benefit from an adjustable rear axle differential and variable braking bias.

The various phenomena explored in this work are summarized in Figure 10. It shows a *G-G Diagram* for each of the three powertrain configurations. The results are taken from the Barcelona track optimizations, and the convex hull is highlighted to show the performance extremes throughout the lap. It is immediately clear that the vehicle with individual thrust control can sustain the highest magnitude of acceleration at any combination of lateral and longitudinal acceleration. The difference in performance to the four-wheel-drive vehicle with a single thrust control is particularly visible in pure deceleration and combined deceleration. However, the four-wheel-drive vehicle with individual thrust controls can also sustain slightly higher pure lateral acceleration and pure longitudinal acceleration through optimized torque vectoring. The two-wheel-drive vehicle performs similarly to the four-wheel-drive vehicle with a

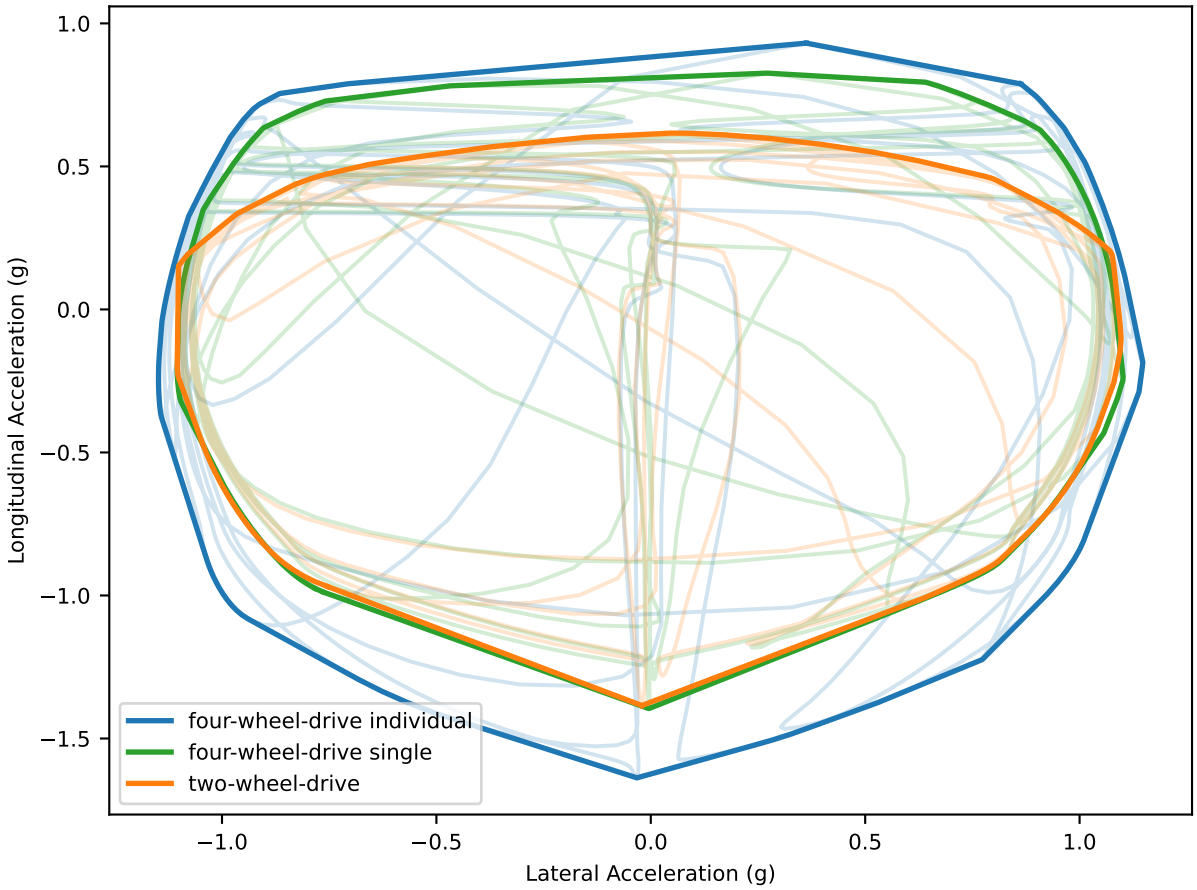

Figure 10. G-G Diagrams for each of the three powertrain configurations on the Barcelona track

single thrust control, except for lower (combined) longitudinal acceleration. This is expected, given that they share the same fixed braking bias. The diagram shows how individual control over the wheel torques can substantially increase performance over other configurations.

4. Conclusions

This work analyzes the minimum lap time optimal control of vehicles with in-hub motors and actively controlled aerodynamics. The approach is to formulate a minimum lap time optimal control problem, modifying state equations of a 3-DOF vehicle model to accommodate the additional controls. The problem is transcribed within OpenMDAO Dymos and solved with IPOPT.

We find significant lap time reduction for a four-wheel-drive in-hub motor configuration over a two-wheel-drive configuration. The lap time reduction was 4% for the Barcelona GP track. For each of the three propulsion configurations, active control over the aerodynamics yields a similar improvement in lap time, roughly 1%.

The optimal trajectory of the four-wheel-drive vehicle with individual thrust controls yields lower minimum cornering speeds than a two-wheel-drive vehicle, indicating that it trades some of its available lateral tire force for additional longitudinal force.

It operates each tire close to the grip limit, enabling much quicker acceleration and deceleration.

When comparing the use of the rear wing flap, we find that the two-wheel-drive vehicle lowers the flap to the maximum downforce and drag configuration earlier than the four-wheel-drive vehicle and raises it to the low drag configuration later. This means that the four-wheel-drive vehicle sustains similar cornering performance by modulating the thrust responses of each wheel without relying on the additional rear wing downforce. Overall, both innovations are beneficial from a minimum lap time perspective.

When designing and implementing complex subsystems such as individually controlled in-hub motors or actively controlled aerodynamic surfaces, the interactions between the vehicle and its subsystems must be designed in unison. This work shows how trajectory optimization can be used to guide the development of control strategies for these systems while considering the fundamental vehicle dynamics. To maximize the performance of racing vehicles, analysis such as presented in this work is a crucial component of the design cycle.

5. References

References

[1] Alessandro Pietro Bardelli. Automatic Racing Lines Generation For High-End Car Games. 2009.

[2] Yan Chen and Junmin Wang. Energy-efficient control allocation with applications on planar motion control of electric ground vehicles. *Proceedings of the American Control Conference*, (August):2719–2724, 2011. ISSN 07431619. .

[3] Fabian Christ, Alexander Wischnewski, Alexander Heilmeier, and Boris Lohmann. Time-optimal trajectory planning for a race car considering variable tyre-road friction coefficients. *Vehicle System Dynamics*, 0(0):1–25, 2019. ISSN 17445159. . URL `https://doi.org/00423114.2019.1704804`.

[4] Nicola Dal Bianco, Enrico Bertolazzi, Francesco Biral, and Matteo Massaro. Comparison of direct and indirect methods for minimum lap time optimal control problems. *Vehicle System Dynamics*, 57(5):665–696, 2019. ISSN 17445159. . URL `https://doi.org/10.1080/00423114.2018.1480048`.

[5] Ricardo De Castro, Mara Tanelli, Rui Esteves Araújo, and Sergio M. Savaresi. Minimum-time manoeuvring in electric vehicles with four wheel-individual-motors. *Vehicle System Dynamics*, 52(6):824–846, 2014. ISSN 17445159. . URL `https://doi.org/10.1080/00423114.2014.902973`.

[6] Leonardo De Novellis, Aldo Sorniotti, and Patrick Gruber. Wheel torque distribution criteria for electric vehicles with torque-vectoring differentials. *IEEE Transactions on Vehicular Technology*, 63(4):1593–1602, 2014. ISSN 00189545. .

[7] Justin S. Gray, John T. Hwang, Joaquim R.R.A. Martins, Kenneth T. Moore, and Bret A. Naylor. OpenMDAO: an open-source framework for multidisciplinary design, analysis, and optimization. *Structural and Multidisciplinary Optimization*, 59(4):1075–1104, 2019. ISSN 16151488. .

[8] Alexander Heilmeier, Alexander Wischnewski, Leonhard Hermansdorfer, Johannes Betz, Markus Lienkamp, and Boris Lohmann. Minimum curvature trajectory planning and control for an autonomous race car. *Vehicle System Dynamics*, 58(10):1497–1527, 2020. ISSN 17445159. . URL `https://doi.org/10.1080/00423114.2019.1631455`.

[9] W. Hirschberg, G. Rill, and H. Weinfurter. Tire model TMeasy. *Vehicle System Dynamics*, 45(SUPPL. 1):101–119, 2007. ISSN 00423114. .

[10] Mehdi Imani Masouleh and David J.N. Limebeer. Optimizing the Aero-Suspension Interactions in a Formula One Car. *IEEE Transactions on Control Systems Technology*, 24 (3):912–927, 2016. ISSN 10636536. .

[11] David Jeffrey, Xin Zhang, and David W. Hurst. Some aspects of the aerodynamics of gurney flaps on a double-element wing. *Journal of Fluids Engineering, Transactions of the ASME*, 123(1):99–104, 2001. ISSN 1528901X. .

[12] D. J.N. Limebeer and G. Perantoni. Optimal Control of a Formula One Car on a Three-Dimensional Track - Part 2: Optimal Control. *Journal of Dynamic Systems, Measurement and Control, Transactions of the ASME*, 137(5):1–13, 2015. ISSN 15289028. .

[13] D. J.N. Limebeer, G. Perantoni, and A. V. Rao. Optimal control of Formula One car energy recovery systems. *International Journal of Control*, 87(10):2065–2080, 2014. ISSN 13665820. . URL http://dx.doi.org/10.1080/00207179.2014.900705.

[14] R. Lot and F. Biral. *A curvilinear abscissa approach for the lap time optimization of racing vehicles*, volume 19. IFAC, 2014. ISBN 9783902823625. . URL http://dx.doi.org/10.3182/20140824-6-ZA-1003.00868.

[15] M. Massaro and D. J.N. Limebeer. Minimum-lap-time optimisation and simulation. *Vehicle System Dynamics*, 59(7):1069–1113, 2021. ISSN 17445159. .

[16] James Patrick Merkel. Development of Multi-Element Active Aerodynamics for the Formula Sae Car. (December), 2013. URL https://uta-ir.tdl.org/uta-ir/bitstream/handle/10106/24176/Merkel{_}uta{_}2502M{_}12503.pdf?sequence=1.

[17] Hans B. Pacejka and Egbert Bakker. The magic formula tyre model. *Vehicle System Dynamics*, 21(sup1):1–18, 1992. ISSN 17445159. .

[18] Giacomo Perantoni and David J.N. Limebeer. Optimal control for a Formula One car with variable parameters. *Vehicle System Dynamics*, 52(5):653–678, 2014. ISSN 17445159. . URL https://doi.org/10.1080/00423114.2014.889315.

[19] H. Scherenberg. Mercedes-benz racing design and cars experience. *SAE Technical Papers*, 66:414–420, 1958. ISSN 26883627. .

[20] Tadeas Sedlacek, Dirk Odenthal, and Dirk Wollherr. Minimum-time optimal control for battery electric vehicles with four wheel-independent drives considering electrical overloading. *Vehicle System Dynamics*, 0(0):1–26, 2020. ISSN 17445159. . URL https://doi.org/00423114.2020.1823004.

[21] R. S. Sharp and Huei Peng. Vehicle dynamics applications of optimal control theory. *Vehicle System Dynamics*, 49(7):1073–1111, 2011. ISSN 00423114. .

[22] Blake Siegler and David Crolla. Lap time simulation for racing car design. *SAE Technical Papers*, (February), 2002. ISSN 26883627. .

[23] Blake Siegler, Andrew Deakin, and David Crolla. Lap time simulation: Comparison of steady state, quasi-static and transient racing car cornering strategies. *SAE Technical Papers*, (724), 2000. ISSN 26883627. .

[24] E. N. Smith, E. Velenis, D. Tavernini, and D. Cao. Effect of handling characteristics on minimum time cornering with torque vectoring. *Vehicle System Dynamics*, 56(2):221–248, 2018. ISSN 17445159. . URL https://doi.org/10.1080/00423114.2017.1371771.

[25] Davide Tavernini, Matteo Massaro, Efstathios Velenis, Diomidis I. Katzourakis, and Roberto Lot. Minimum time cornering: The effect of road surface and car transmission layout. *Vehicle System Dynamics*, 51(10):1533–1547, 2013. ISSN 00423114. .

[26] M. Veneri and M. Massaro. A free-trajectory quasi-steady-state optimal-control method for minimum lap-time of race vehicles. *Vehicle System Dynamics*, 58(6):933–954, 2020. ISSN 17445159. .

[27] Andreas Wächter and Lorenz T. Biegler. *On the implementation of an interior-point filter line-search algorithm for large-scale nonlinear programming*, volume 57. 2006. ISBN 1010700405.

[28] W. J. West and D. J.N. Limebeer. Optimal tyre management for a high-performance race car. *Vehicle System Dynamics*, 0(0):1–19, 2020. ISSN 17445159. . URL https://doi.org/00423114.2020.1802047.